Chapter 4
Dynamics of Formation of Massive Stars

https://doi.org/10.1017/S1743921323002326 Published online by Cambridge University Press

Cosmic Masers: Proper Motion toward the Next-Generation Large Projects
Proceedings IAU Symposium No. 380, 2024
T. Hirota, H. Imai, K. Menten, & Y. Pihlström, eds.
doi:10.1017/S1743921323002326

Evolutionary Trends in Star Formation

J. S. Urquhart

Centre for Astrophysics and Planetary Science, University of Kent, Canterbury, CT2 7NH, UK. email: j.s.urquhart@kent.ac.uk

Abstract. Over the past 20 years, the Galactic plane has been surveyed at high resolution at wavelengths from 1 micron through to 20 cm. The combination of these surveys has produced large samples of deeply embedded young stars located across the Galactic disc. These continuum surveys are complemented by spectral line surveys of thermal, radio recombination, and molecular maser (OH, H_2O, CH_3OH) lines. The identified sources cover the whole range of evolutionary stages in the star formation process, allowing the physical properties of these stages to be measured. This information has been used to calculate the star formation efficiency and star formation rate of the Milky Way and to evaluate the impact of environment and location within the disc. This review provides an overview of some of the most significant studies in recent years and discusses how the evolutionary sequence has been used to investigate the correlation of other star formation tracers and maser associations.

Keywords. Masers, star: formation, ISM: molecules, ISM: surveys

1. Introduction

Massive stars ($>8\,M_\odot$ and $10^3\,L_\odot$) play an important role in many astrophysical processes and in shaping the morphological, dynamical and chemical structure of their host galaxies (Kennicutt & Evans 2012). These stars have a profound impact on their local environment through powerful outflows, strong stellar winds and copious amounts of optical/far-UV radiation, which shape the interstellar medium (ISM) and regulate star formation, and ultimately governs the evolution of their host galaxy (McKee & Ostriker 2007). During their lives they reprocess huge amounts of material and are responsible for most of the heavy elements in the universe, which are returned to the ISM through stellar winds, and at the ends of their lives, in supernovae explosions. Furthermore, emission from massive stars dominates the light seen from distant galaxies, and therefore, galaxy models are critically dependent on various assumptions that are made about high-mass star formation, such as the star formation rate (SFR; Davies *et al.* 2011) or the universality of the initial mass function (IMF; Kroupa & Weidner 2003), if we are to understand how they evolved over cosmological timescales. Understanding the formation and early evolution of massive stars is therefore a fundamental goal for modern astrophysics.

Studies of external galaxies are generally restricted to studies of global star formation properties integrated over entire complexes (resolution ∼90 pc; Rosolowsky *et al.* 2021) or even entire galaxies (Gao & Solomon 2004). Studies of star formation within our own Galaxy, however, are able to probe star forming regions in far greater detail and the large range of environments available have extragalactic analogues (Kruijssen & Longmore 2013), e.g., the Galactic centre with its extreme UV-radiation and cosmic ray fluxes, intense star formation regions found in the disc (e.g., W43 and W51; often described as "mini-starbursts") and low-metallicity environment found in the outer Galaxy. The Milky Way, therefore, provides our best opportunity to understand the processes involved in massive star formation in both Galactic and extragalactic environments.

Despite their importance our understanding of the initial conditions required, and processes involved, in the formation and early evolution of massive stars, is still rather poor. There are a number of reasons for this: massive stars are rare and relatively few are located closer than a few kpc from the Sun; they form almost exclusively in clusters, making it hard to distinguish between the properties of the cluster and individual members; and they evolve rapidly, reaching the main sequence while still deeply embedded in their natal environment, and consequently, the earliest stages can only be probed at far-infrared and (sub)millimetre wavelengths (see Motte *et al.* 2018 for a review). To overcome these difficulties requires a combination of unbiased multi-wavelength Galactic plane surveys to identify large samples of embedded massive stars and high resolution to study their properties in detail.

Our ability to make significant progress in this field has been dramatically enhanced in recent years with the completion of a large number of Galactic plane surveys that cover the whole wavelength range from the near-infrared to the radio, e.g., UKIDSS (Lucas *et al.* 2008), GLIMPSE (Churchwell *et al.* 2009), Hi-GAL (Molinari *et al.* 2010), ATLASGAL (Schuller *et al.* 2009) and CORNISH (Hoare *et al.* 2012) (see Table 1 for a more comprehensive list). These unbiased surveys provide the large spatial volumes required to address the major problem in studying Galactic massive star formation, its intrinsic rarity. These continuum surveys are complemented by a number of unbiased and targeted spectral line surveys that can constrain the macroscopic properties of star forming environments, e.g., COHRS (Dempsey *et al.* 2013), SEDIGISM (Schuller *et al.* 2021) and MALT90 (Jackson *et al.* 2013).

Combined, these surveys provide a global view of massive star formation and enable the identification and characterisation of statistically significant samples over the full range of evolutionary stages from pre-stellar through to the post-compact HII region stage when the star emerges from its natal clump (see Fig. 1). The availability of these surveys and upgrades of facilities like the Jansky Very Large Array presents an exciting opportunity to make significant progress in our understanding of the formation and evolution of massive stars and their role in driving galaxy evolution.

In this review we will look at the progress that has been made in identifying large samples of embedded high-mass star forming environments over the past 20 years and give an overview of the current state of the art.

2. The Evolutionary Sequence

Most stars form in high-mass star-forming clusters found within the densest parts of giant molecular clouds (Williams & McKee 1997); these are often referred to as clumps. These have volume densities of $10^{4-5}\,\mathrm{cm}^{-3}$, sizes of $\sim$1 pc and masses of 500–1000 $M_{\odot}$ (Urquhart *et al.* 2014b). These dense clumps are initially in a quiescent state (starless) but are gravitationally bound and continue to accrete material from their surroundings that flows in along filamentary networks. These clumps become gravitationally unstable and begin to collapse, resulting in the formation of a protostar, which will become visible first at far-infrared wavelengths (e.g., 70 μm), then at mid-infrared and near-infrared wavelengths as it accretes more material and becomes hotter, resulting in the peak of its spectral energy distribution (SED) shifting to shorter wavelengths. This mid-infrared stage is often referred to as the massive young stellar object (MYSO) stage and precedes the stars arriving on the main sequence stars, which is indicated by the formation of an HII region.

Figure 1 presents a schematic that shows the main evolutionary stages and the wavelength ranges that the various stages are detectable. We use this to identify 4 observationally distinct evolutionary stages: 1) the quiescent stage is far-infrared quiet and

https://doi.org/10.1017/S1743921323002326 Published online by Cambridge University Press

Table 1. Summary of Galactic plane surveys.

Survey	Wavelength	Beam ($''$)	ℓ Coverage ($^\circ$)	b Coverage ($^\circ$)	Probe	Reference
IPHAS	Hα	1.7	$30^\circ < l < 210^\circ$	$\|b\| < 5^\circ$	Nebulae & stars	Drew *et al.* (2005)
UKIDSS	JHK	0.8	$-2^\circ < l < 230^\circ$	$\|b\| < 1^\circ$	Stars, Nebulae	Lucas *et al.* (2008)
VVV	ZYJHK	0.8	$-65^\circ < l < 10^\circ$	$\|b\| < 2^\circ$	Nebulae Nebulae	Minniti *et al.* (2010)
GLIMPSE	4-8	2	$-65^\circ < l < 65^\circ$	$\|b\| < 1^\circ$	Stars, Hot Dust	Churchwell *et al.* (2009)
MSX	8-21	18	All	$\|b\| < 5^\circ$	Warm Dust	Price *et al.* (2001)
MIPSGAL	24,70	6, 20	$-65^\circ < l < 65^\circ$	$\|b\| < 1^\circ$	Warm Dust	Carey *et al.* (2009)
AKARI	50-200	30-50	All sky		Cool Dust	White *et al.* (2009)
Hi-GAL	70-500	10-34	All	$\|b\| < 1^\circ$a	Cool Dust	Molinari *et al.* (2010)
JPS	450,850	8-14	$10^\circ < l < 60^\circ$	$\|b\| < 1^\circ$	Cool Dust	Moore *et al.* (2015)
ATLASGAL	850	19	$-60^\circ < l < 60^\circ$	$\|b\| < 1.5^\circ$	Cool Dust	Schuller *et al.* (2009)
BOLOCAM	1100	33	$-10^\circ < l < 90^\circ$	$\|b\| < 0.5^\circ$	Cool Dust	Aguirre *et al.* (2011)
GRS	^{13}CO 1-0	46	$18^\circ < l < 56^\circ$	$\|b\| < 1^\circ$	Molecular Gas	Jackson *et al.* (2006)
MMB	6.7 GHz	192b	$-180^\circ < l < 60^\circ$	$\|b\| < 2^\circ$	Methanol Masers	Green (2009)
HOPS	22 GHz	132b	$-180^\circ < l < 60^\circ$	$\|b\| < 2^\circ$	Water Masers	Walsh *et al.* (2011)
OH	1.6 GHz	$\sim$10	$-45^\circ < l < 45^\circ$	$\|b\| < 3^\circ$	Hydroxyl Masers	Sevenster *et al.* (2001)
CORNISH -North	6 cm	1.5	$10^\circ < l < 65^\circ$	$\|b\| < 1^\circ$	Compact Ionized Gas	Hoare *et al.* (2012)
CORNISH -South	6 cm	3	$300^\circ < l < 350^\circ$	$\|b\| < 1^\circ$	Ionized Ionized Gas	Irabor *et al.* (2023)
GLOSTAR	6 cm	1.5-20	$-2^\circ < l < 60^\circ$	$\|b\| < 1^\circ$	Compact Ionized Gas	Brunthaler *et al.* (2021)
THOR	20 cm	20	$14.4^\circ < l < 67.4^\circ$	$\|b\| < 1.25^\circ$	Atomic and Ionized Gas	Beuther *et al.* (2016)
S/V/CGPS	21 cm	60	$-107^\circ < l < 147^\circ$	$\|b\| < 1.3^\circ$	Gas Gas	Stil *et al.* (2006)
MAGPIS	20 cm	5	$5^\circ < l < 48^\circ$	$\|b\| < 0.8^\circ$	Diffuse Ionized Gas	Helfand *et al.* (2006)
MGPS-2	35 cm	45	$-115^\circ < l < 0^\circ$	$\|b\| < 10^\circ$	Diffuse Ionized Gas	Murphy *et al.* (2007)

Notes: This table is a modified version of the table 1 of Hoare *et al.* 2012.

so precedes the formation of any protostellar objects; 2) the protostellar stage is far-infrared bright, indicating the formation of a protostellar object, but that is not yet evolved enough to be mid-infrared bright; 3) the MYSO stage, where the embedded protostellar object is luminous ($> 10^3\,L_\odot$; Wynn-Williams 1982) and hot enough to be detected at mid-infrared wavelengths but has not yet started to form a detectable HII region; and finally 4) the HII region stage when the star has joined the main sequence and begun to ionize its surrounding natal gas and can now be detected at radio wavelengths (See Figure 2 for spectral energy distributions of the four evolutionary stages).

https://doi.org/10.1017/S1743921323002326 Published online by Cambridge University Press

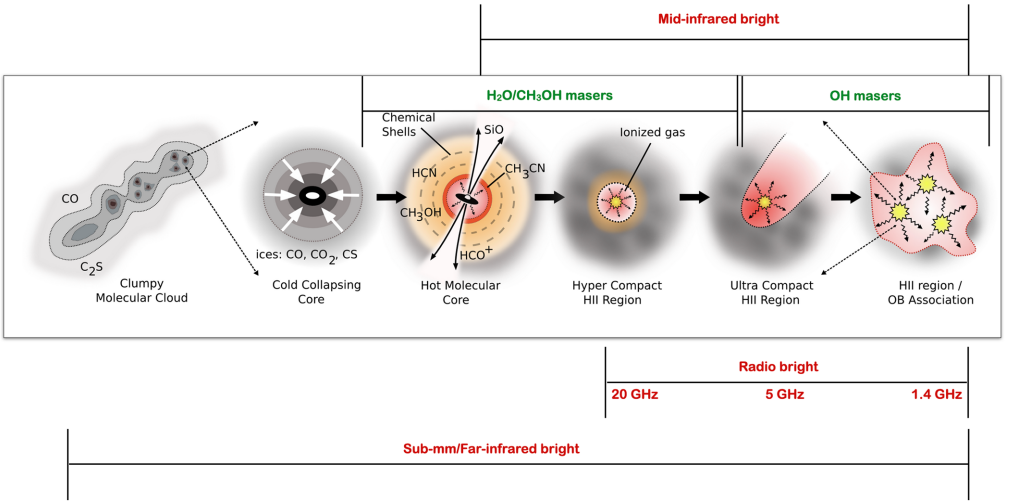

Figure 1. Schematic for the evolutionary sequence of massive star formation. Infrared and radio surveys are sensitive to the more evolved stages shown to the right while submillimetre surveys are sensitive to all evolutionary stages. The greyscale indicates the distribution of cold gas and dust with the darker areas corresponding to denser regions. The protostellar objects are indicated by the yellow circles, warmer gas by the orange colouring and the hotter ionized gas is shown in red. Molecular lines used to trace the properties of the molecular gas in different stages are also noted. The red labels and associated horizontal lines show the wavelengths and time ranges that different stages are observable, and the green labels indicate the maser associations. Image Credit: Cormac Purcell.

3. Legacy of the IRAS

Given that high-mass star formation occurs deep inside dense clumps, behind hundreds of magnitudes of visual extinction, all of the earliest stages are inaccessible from ground based telescopes. Progress in this area only became possible with the launch of the Infrared Astronomical Satellite (IRAS) in 1983. IRAS surveyed 96% of the sky in 4 mid- and far-infrared photometric bands (12, 25, 60 and 100 μm) detecting more than 250,000 sources (IRAS Point Source Catalogue or PSC Version 2; Beichman *et al.* 1988) that could be used to develop colour selection criteria to identify embedded high-mass young stellar objects (e.g., Campbell *et al.* 1989; Chan *et al.* 1996). These colour selected samples are not able to distinguish between MYSO and the more evolved HII region stages, however, the latter stage is bright at radio wavelengths. Work by Wood & Churchwell (1989) and Kurtz *et al.* (1994) with the VLA was able to separate these two stages, resulting in the identification of ∼100 ultracompact (UC) HII regions and allowing their physical properties to be characterised.

Molinari *et al.* (1996) applied colour cuts to the IRAS PSC and identified 260 objects with properties consistent with being embedded high-mass protostars. Approximately half of which have colours consistent with being UC HII regions (according to the work of Wood & Churchwell 1989); they refer to these as the 'High' group with the remaining sources referred to as the 'Low' group, which have been the starting point for many follow-up studies (e.g., Wu *et al.* 2006). Sridharan *et al.* (2002) used data from a higher spatial resolution imaging of the original IRAS data (HIRES; Aumann *et al.* 1990) to identify a sample of high-mass protostellar objects and used molecular line and radio continuum data to characterise the sample (Beuther *et al.* 2002) and to exclude more evolved HII regions.

https://doi.org/10.1017/S1743921323002326 Published online by Cambridge University Press

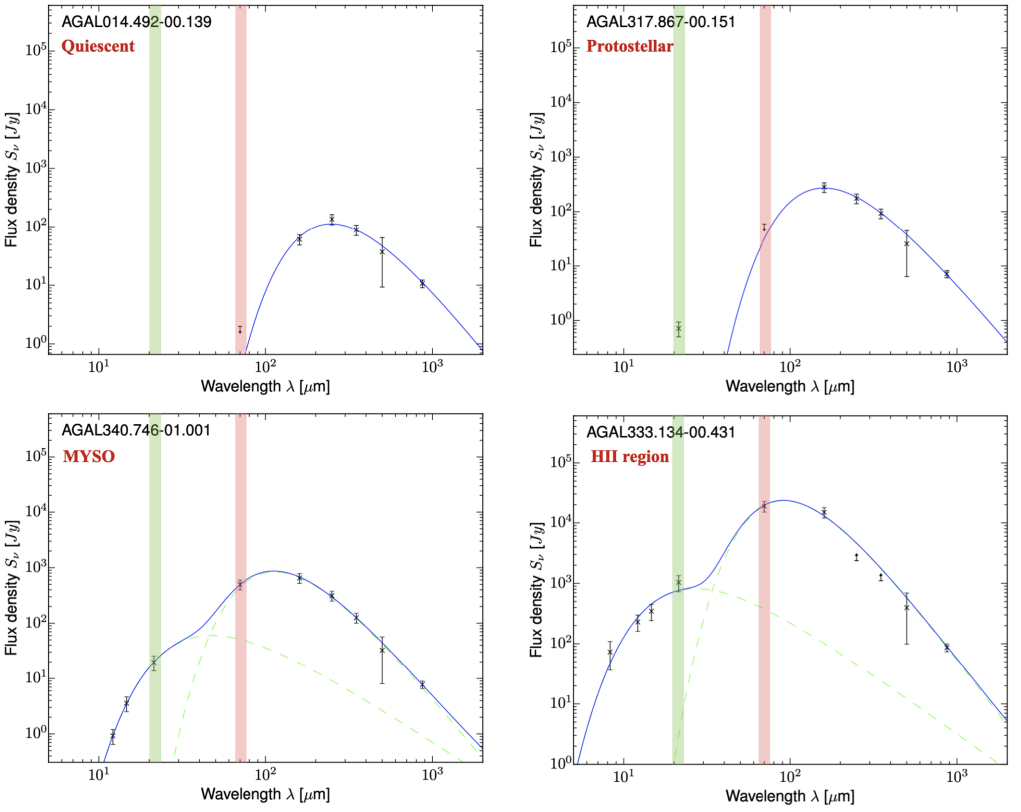

Figure 2. Examples of spectral energy distributions (SEDs) from the four evolutionary stages described in the text. These are taken from the ATLASGAL survey and have been adapted from figure 7 of König *et al.* (2017). The source names and evolutionary stage are given in the upper left corner of each plot. The mid-infrared flux values have been drawn from the MSX, WISE or MPISGAL surveys while the far-infrared and submillimetre fluxes (70-500 μm) have been drawn from HiGAL and the 870 μm comes from ATLASGAL. The blue curve shows the results of greybody fits to the photometric points (a single component for the quiescent and protostellar clumps and two components to the MYSO and HII region associated clumps). The red and green vertical lines indicate wavelengths that are used to distinguish between quiescent and protostellar clumps, and protostellar and more evolved clumps (i.e., those hosting MYSOs and HII regions). Image Credit: Carsten König.

These early studies were limited by the IRAS angular resolution ($\sim 2'$), so focus on bright isolated sources and tended to be biased away from intense star formation regions and from the Galactic mid-plane where source confusion is high. In the next section we will discuss a survey that took advantage of the higher-resolution mid-infrared photometry provided by the Midcourse Space Experiment (MSX) to produce a large and well-selected catalogue of MYSOs and UC HII regions.

4. The Red MSX Source (RMS) Survey

The Red MSX Source (RMS) survey is a systematic search of the entire Galaxy mid-plane for MYSOs and HII regions. This survey makes use of the higher resolution provided by the MSX satellite (Price *et al.* 2001) to conduct a large comprehensive search for young embedded high-mass stars. This reduces the biases affecting the early studies based on IRAS data.

https://doi.org/10.1017/S1743921323002326 Published online by Cambridge University Press

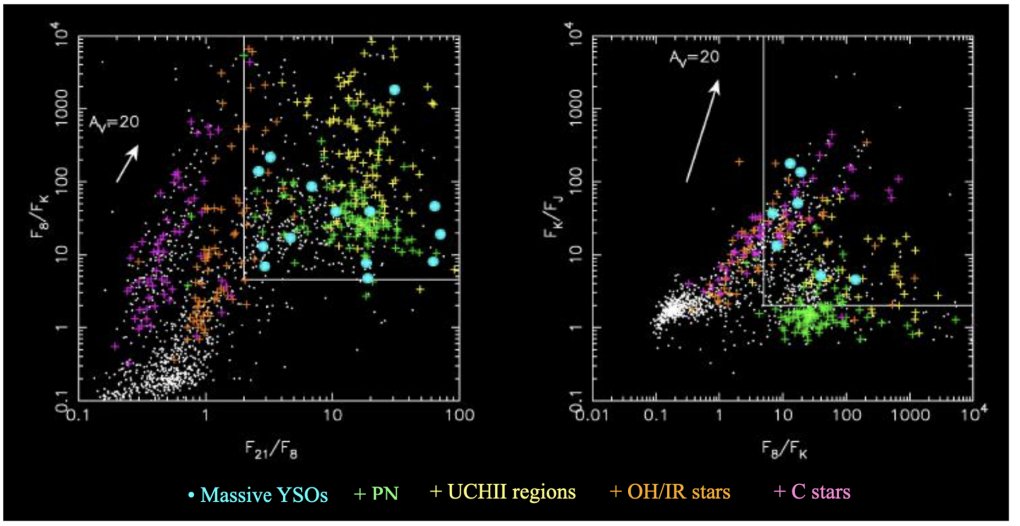

Figure 3. Colour-colour plots showing the distribution of different kinds of objects encountered in the search for embedded high-mass protostellar objects. The colours indicate the ratios of the fluxes at different wavelengths where 8 and 21 refer to the MSX fluxes at 8 and 21 μm and the J, H, K refer to the 2MASS magnitudes. The regions enclosed by the white boxes are the regions of the colour-colour space where the previously identified MYSOs are located and the selection criteria used for identifying the RMS sample of MYSO candidates. Image Credit: Stuart Lumsden.

The MSX was launched in 1996 and surveyed the entire Galactic plane ($|b| < 5°$) in four mid-infrared spectral bands between 6 and 25 μm at a spatial resolution of $\sim$18″ (Price *et al.* 2001). The resulting point source catalogue contains 440,483 sources (Egan *et al.* 2003). The RMS team started by selecting MYSOs that have similar mid-infrared colours as embedded high-mass protostars identified in the previous IRAS studies. To this they added near-infrared photometry from the 2MASS survey (Skrutskie *et al.* 2006) to exclude more evolved sources. These colour cuts and the visual inspection of the images to eliminate extended sources resulted in the identification of $\sim$2000 MYSO candidates (Lumsden *et al.* 2002).

Figure 3 shows the colour-colour plots used to identify the MYSO candidates by the RMS team. These plots demonstrate how effective these colour criteria are at excluding evolved stars from the sample, however, they are not able to remove the contaminating sources completely or to differentiate between MYSOs or HII regions. To accomplish this required a comprehensive multi-wavelength campaign of follow-up observations including near-infrared spectroscope (Clarke *et al.* 2006; Wheelwright *et al.* 2010; Ilee *et al.* 2013; Cooper *et al.* 2013) mid-infrared continuum (Mottram *et al.* 2007), molecular line (Urquhart *et al.* 2007b, 2008, 2011), and radio continuum (Urquhart *et al.* 2007a, 2009).

These efforts have resulted in the production of a sample of approximately 600 YSOs, 110 of which have luminosities above 20,000 $L_\odot$ and are therefore considered genuine MYSOs, and a similar number of UC HII regions (Lumsden *et al.* 2013; Urquhart *et al.* 2014a). This is the largest and most complete sample of MYSOs and UC HII regions produced to date.

5. Radio Continuum Surveys

Radio continuum surveys are an indispensable part of defining an evolutionary sequence for high-mass star formation. Arguably, this is not a formation stage given that

https://doi.org/10.1017/S1743921323002326 Published online by Cambridge University Press

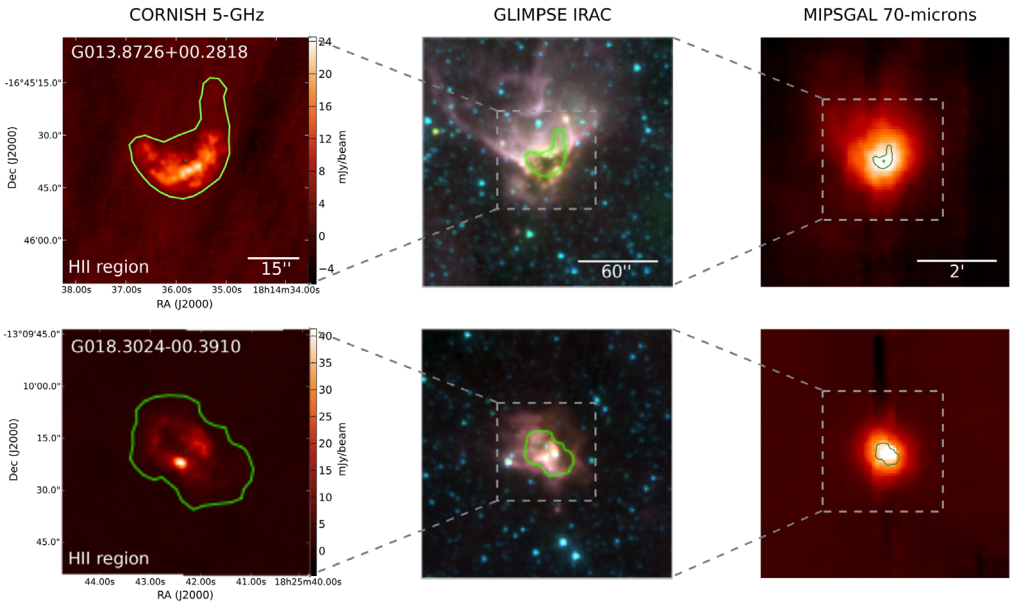

Figure 4. Examples of two UC HII regions identified in the CONRISH-North survey. This has been adapted from figure 22 from Purcell *et al.* (2013). The left panels show the radio emission and the green polygon the area over which the flux is integrated. The middle panels are three colour composite images showing the mid-infrared environment and the right panels show the far-infrared emission from MIPSGAL. Image Credit: Cormac Purcell.

accretion has been terminated and the star has arrived on the main sequence. However, the detection of the radio emission from the ionized gas surrounding the newly formed OB star allow MYSOs and more evolved UC HII regions to be separated, which is not possible from the infrared emission alone. For this reason, it is worth reviewing the contribution of radio surveys have made to the development of the evolutionary sequence.

There are several HII region stages that have been identified. The hypercompact (HC) HII regions are the most compact with diameter < 0.03 pc and densities $n_e > 10^6$ cm^{-3} (Kurtz & Hofner 2005) and are optically thick below 10 GHz (where most radio surveys have been conducted). These expand into the ultracompact (UC) HII region stage defined as having diameters of < 0.1 pc and densities $n_e > 10^4$ cm^{-3} (Wood & Churchwell 1989). The expansion of the HII region continues and the electron density continues to decrease through the compact HII region stage ($n_e > 10^4$ cm^{-3} and diameter > 0.1 pc; Wood & Churchwell 1989) until it breaks out of its natal cloud and becomes optically visible, at which point it is described as a classical HII region. All of the HII region stages are unlikely to be distinct stages but rather observationally determined size scales on a continuum (Hoare *et al.* 2007).

The HII region most commonly associated with the early stages of high-mass star formation is the UC HII region stage. At this point in the HII regions evolution, its electron density has dropped to a point that the nebula has become optically thin at 5 GHz and this frequency is where most radio surveys have been targeted (e.g., CORNISH. Hoare *et al.* 2012; GLOSTAR. Brunthaler *et al.* 2021). The HC HII region stage is the earliest manifestation of a HII region, however, this is thought to be very short-lived (only 21 have been detected; Yang *et al.* 2021) and the higher frequency (>10-20 GHz) and small beam makes the large systematic survey needed to search for these unfeasible with current telescopes.

https://doi.org/10.1017/S1743921323002326 Published online by Cambridge University Press

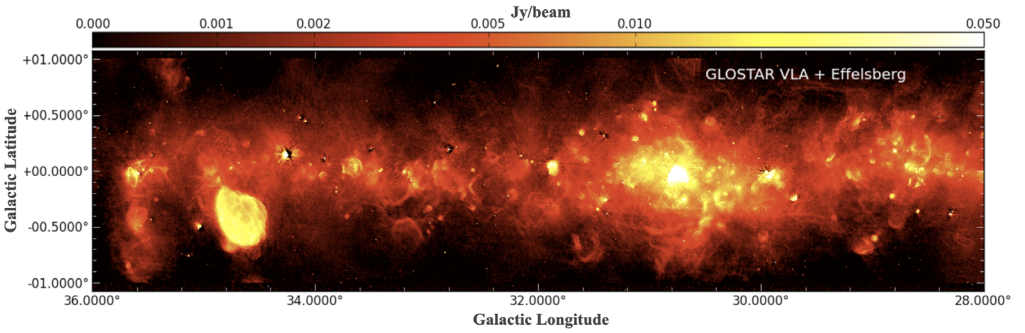

Figure 5. Radio continuum image of the GLOSTAR pilot region in the range $28^\circ < \ell < 36^\circ$. This image has been produced by combining of the VLA D configuration and the Effelsberg single-dish continuum data. This image has been adapted from figure 5 of Brunthaler *et al.* (2021). Image Credit: Andreas Brunthaler.

The CORNISH survey consists of two parts: CORNISH-North conducted with the Very Large Array (VLA) and CORNISH-South conducted with the Australia Telescope Compact Array (ATCA). These two surveys have identified ∼7,000 compact radio sources (Purcell *et al.* 2013; Irabor *et al.* 2023) of which ∼800 have been classified as compact HII regions including 494 that have been classified as UC HII regions (Irabor *et al.* 2023; Kalcheva *et al.* 2018). Figure 4 shows two examples of HII regions detected in the CORNISH-North survey region (Purcell *et al.* 2013).

The GLOSTAR survey is a new VLA survey that is covering most of the 1st Galactic quadrant ($-2^\circ < \ell < 60^\circ$ and $|b| < 1^\circ$) and Cygnus X star formation region ($76^\circ < \ell < 83^\circ$ and $-1^\circ < b < 2^\circ$) in the frequency range 4-8 GHz and the Effelsberg 100-m telescope (Brunthaler *et al.* 2021). The image resulting from the combination of the VLA D-array and Effelsberg data of the pilot region is shown in Fig. 5. The setup includes spectral windows covering the 6.7 GHz methanol maser transition (Ortiz-León *et al.* 2021; Nguyen *et al.* 2022), formaldehyde and radio recombination lines. Analysis of these data is still in the early stages but results are already starting to emerge (e.g., Medina *et al.* 2019; Nguyen *et al.* 2021; Dokara *et al.* 2021; Dzib *et al.* 2023) that demonstrate the impact this survey will have in the future.

6. Dust Continuum Surveys

The radio and infrared surveys discussed so far have been very successful in identifying large well-selected samples of MYSOs and UC HII regions across the Galactic mid-plane. However, these only provide details on already quite evolved stages in the high-mass star formation process and completely miss the very earliest pre-stellar and protostellar stages. Early attempts to probe these younger evolutionary stages was led by SIMBA on the SEST and SCUBA on the JCMT (e.g., Faúndez *et al.* 2004; Hill *et al.* 2005; Thompson *et al.* 2006). These resulted in the detection of hundreds of dense clumps including many starless clumps, however, they were often made towards MYSOs and UC HII regions identified from studies of IRAS data and so suffer from the same problems described earlier.

ATLASGAL traces dust emission at 870 μm providing the first unbiased survey of the inner Galactic disk (Schuller *et al.* 2009; see Fig. 6 for survey coverage and mass sensitivity). The survey has an angular resolution of $\sim 18''$ and sensitivity of 60 mJy beam^{-1}. The dust emission is optically thin at this frequency and so ATLASGAL is able to probe all evolutionary stages associated with high-mass star formation (see Figure 1).

https://doi.org/10.1017/S1743921323002326 Published online by Cambridge University Press

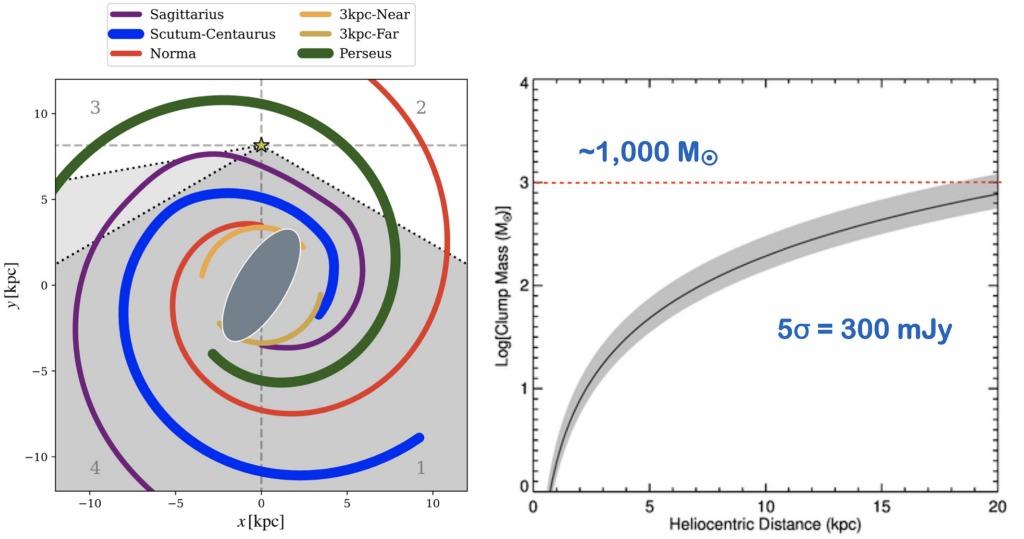

Figure 6. Left: ATLASGAL coverage of the inner Galactic plane. The dark grey shows the initial survey region ($-1.5^\circ < b < 1.5^\circ$) and the light grey the outer Galaxy extension ($-2^\circ < b < 1^\circ$). The spiral arms and the positon and orientation of the Galactic bar are included to show the structures covered in the survey. The position of the Sun is indicated by the yellow star symbol and the numbers in the corners show the Galactic quadrants. Right: Corresponding mass sensitivity as a function of heliocentric distance. The black curve shows the 5σ mass sensitivity as a function of heliocentric distance assuming a dust temperature of 20 K, the grey shading on either side corresponds to an temperature uncertainty of ± 5 K. The dashed horizontal line shows the clump mass completeness limit for ATLASGAL.

A catalogue of ∼10,000 dense clumps (Contreras *et al.* 2013; Urquhart *et al.* 2014c; Csengeri *et al.* 2014) has been identified from the survey maps and their properties have been fully characterised. Their distances are taken from the literature where available, and radial velocities obtained from the follow-up molecular line observation (Wienen *et al.* 2012; Giannetti *et al.* 2013; Csengeri *et al.* 2016; Kim *et al.* 2017; Wienen *et al.* 2018) have been used to determine kinematic distances (Wienen *et al.* 2015; Urquhart *et al.* 2018) for the rest of the clumps. The SED fits to the photometry are used to determine the luminosities and dust temperatures (König *et al.* 2017; see Fig. 2), which is in turn used to determine the clump masses, column and volume densities (Urquhart *et al.* 2022).

As the first step towards defining an evolutionary sample, the ATLASGAL catalogue was cross-matched with the CORNISH-North catalogue (Purcell *et al.* 2013), the Methanol Multibeam (MMB) survey (Green 2009)† and the RMS survey (Lumsden *et al.* 2013) to identify clumps associated with previously identified high-mass protostars (MYSOs and UC HII regions; Urquhart *et al.* 2013b,a, 2014b). These comparisons identified a sample of ∼1400 high-mass star-forming clumps, however, the earliest stages are still missing.

To identify the protostellar and quiescent clumps the 8, 24 and 70 μm images towards the remaining clumps were visually inspected. In Figure 7 an example of these three wavelength images for each of the four evolutionary stages described in Section 2 are presented. A brief summary of the classification scheme used is: clumps that are dark at all wavelengths are classified as quiescent, clumps associated with a 70 μm source but dark

† Methanol maser emission at 6.7 GHz is considered to be exclusively associated with embedded high-mass young stars (Breen *et al.* 2013).

https://doi.org/10.1017/S1743921323002326 Published online by Cambridge University Press

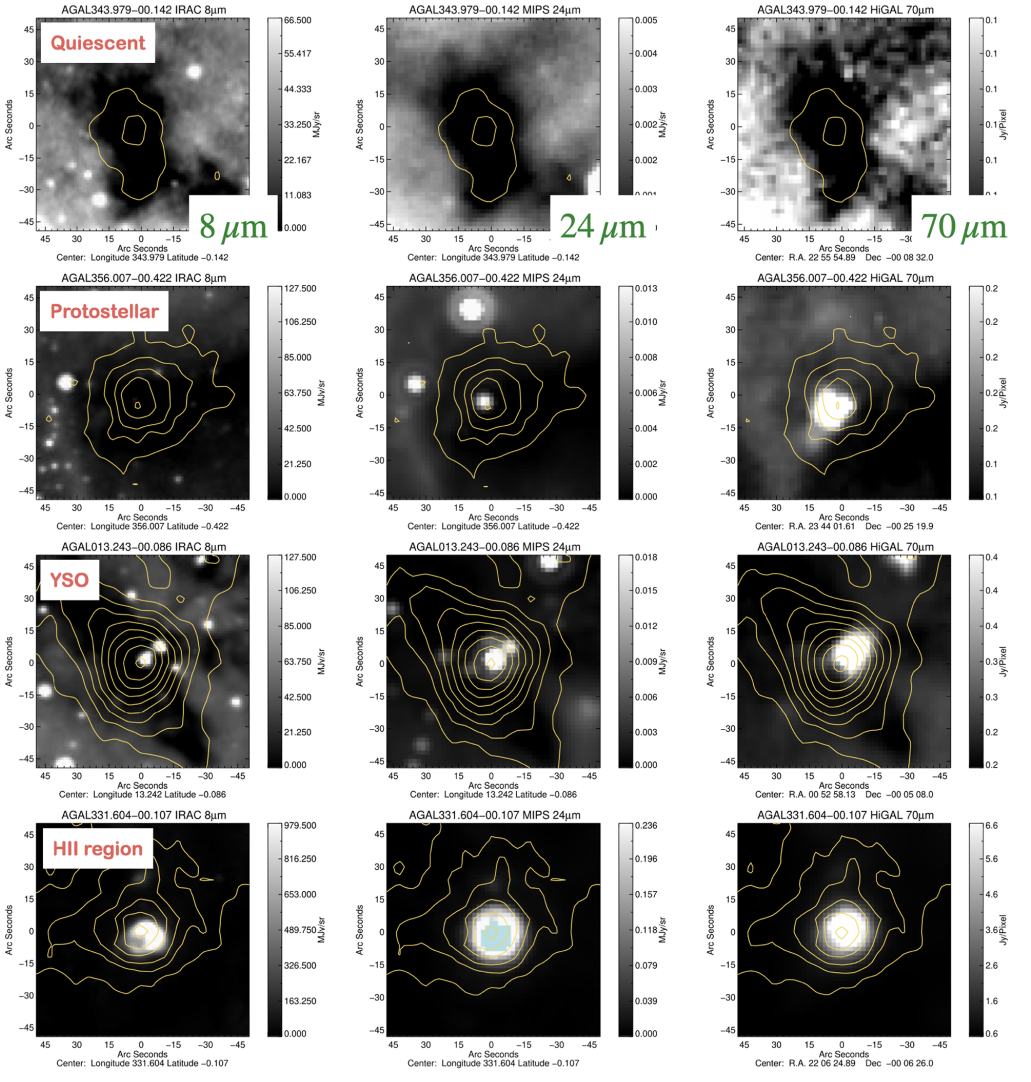

Figure 7. Examples of the images used to classify ATLASGAL sources into one of the four observationally defined evolutionary types. The contours show the distribution of the 870-μm dust emission traced by ATLASGAL. This has been adapted from figure 4 of Urquhart *et al.* (2022).

or weak at 24 μm are classified as protostellar, clumps associated with compact bright point sources at all three wavelengths and not associated with compact radio emission are classified as YSOs, and clumps associated with extended emission in all three images or compact point sources in all three images and radio emission are classified as HII regions.

In total, ∼8,500 clumps have been classified with ∼5,000 clumps being placed in one of the four evolutionary stages (Urquhart *et al.* 2018, 2022). This results in roughly equal number of clumps in each category, indicating that the lifetimes of these stages are also approximately equal. In the next section, we will describe how this evolutionary sample has been used to investigate how the physical properties change during the star formation process.

https://doi.org/10.1017/S1743921323002326 Published online by Cambridge University Press

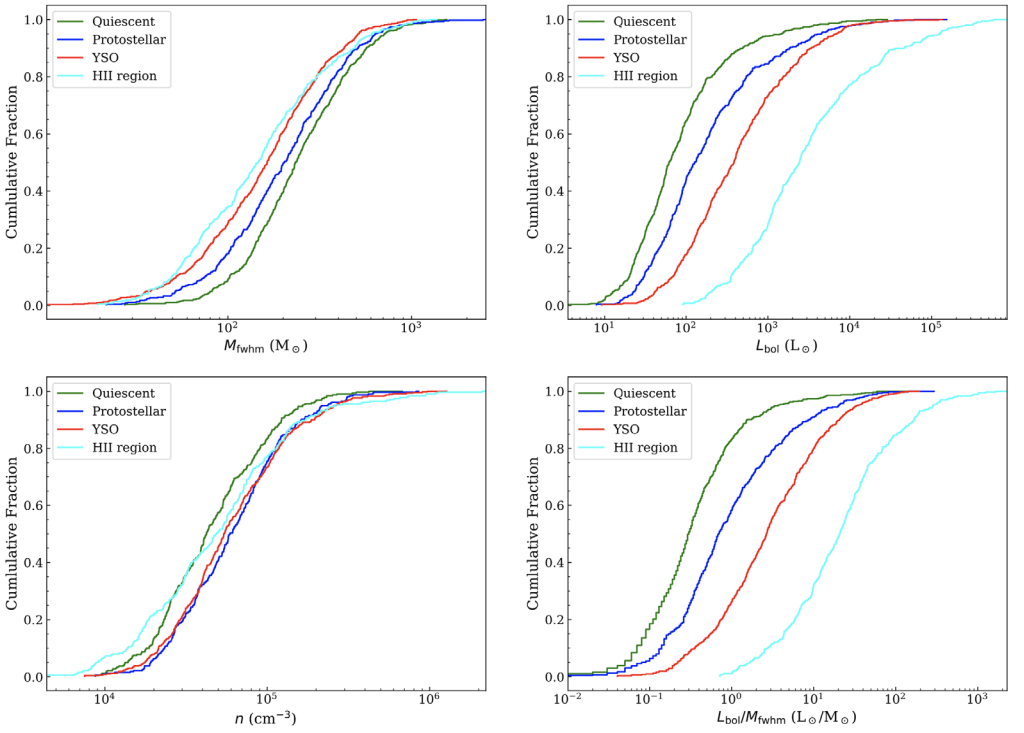

Figure 8. Cumulative distribution functions for the four main evolutionary stages. In the left panels the clump mass and volume densities are shown; these are similar for all stages. In the right panels the bolometric luminosity and the luminosity-to-mass ($L_{\rm bol}/M_{\rm fwhm}$)-ratio are shown; the evolutionary stages are well separated for these parameters making them good evolutionary diagnostics. For all of these plots a distance-limited sample of 2-4 kpc is used to avoid any possible distance bias. This figure has been adapted from figure 7 of Urquhart *et al.* (2022).

7. Towards an Evolutionary Sequence

Figure 8 presents plots comparing the clump mass, density, luminosity and luminosity-to-mass ($L_{\rm bol}/M_{\rm fwhm}$) ratio of a distance-limited sample (2-4 kpc) for the four evolutionary samples discussed in the previous section. The mass is calculated from the 870 μm emission above the half-maximum intensity to avoid a temperature bias due to evolution (see Urquhart *et al.* 2022 for details). No significant difference is revealed for the evolutionary samples in the mass and volume density distributions, however, significant differences are found for the luminosity and $L_{\rm bol}/M_{\rm fwhm}$-ratio, with both of these distributions showing a steady progression to higher values as a function of evolution. The luminosity is expected to increase strongly as the embedded protostar evolves, however, it is also linked to the mass of the protostar so that an evolved low-mass protostar can have a luminosity similar to that of a less-evolved high-mass protostar. The $L_{\rm bol}/M_{\rm fwhm}$-ratio avoids this degeneracy and is therefore considered to be a better indicator of the evolutionary state of clumps (Molinari *et al.* 2008; Urquhart *et al.* 2022).

In left panel of Fig. 9 the $L_{\rm bol}/M_{\rm fwhm}$-ratio for all ATLASGAL clumps and the mean values for the four evolutionary stages is shown. If the observationally identified evolutionary stages represent distinct stages in the star formation process one might expect to see points of inflection and/or jumps in the cumulative distribution function at the transition points of a clump's evolution. However, the distribution is smooth and devoid

https://doi.org/10.1017/S1743921323002326 Published online by Cambridge University Press

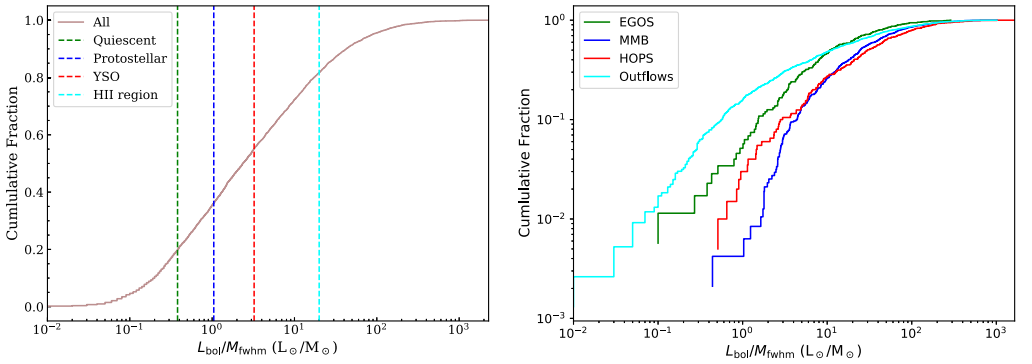

Figure 9. Left: Cumulative distribution function for the $L_{\rm bol}/M_{\rm fwhm}$-ratio of the combined star formation sample (rose curve). The vertical lines indicate the mean of the lognormal distribution of the four evolutionary stages taken from the lower right panel of Figure 8. Right: Cumulative distribution function for the $L_{\rm bol}/M_{\rm fwhm}$-ratio as a function of different star formation tracers (see text for details).

of any features that are coincident with the mean values of $L_{\rm bol}/M_{\rm fwhm}$-ratios for the four evolutionary stages. This lack of any abrupt changes suggests that star formation is a smooth and continuous process. These stages are useful in identifying groups of protostellar objects with similar properties and/or ages, but do not themselves represent fundamentally changes in the physical mechanisms involved.

The ATLASGAL evolutionary sample has been cross-matched with four other star formation tracers to test the validity and to put these other tracers into context. The catalogue of ∼300 extended green objects (EGOs; Cyganowski *et al.* 2008), catalogues of molecular outflows produced by Maud *et al.* (2015); de Villiers *et al.* (2014); Yang *et al.* (2018, 2021), the methanol multibeam (MMB) survey (Green 2009) and water masers identified by HOPS (Walsh *et al.* 2011, 2014) were used. EGOs are identified by their enhanced emission in the 4.5-μm band that contains the rotationally excited H_2 ($v = 0 - 0$, S(9, 10, 11)) and CO ($v = 1 - 0$) band-head lines, which are indicative of outflow activity and active accretion (Cyganowski *et al.* 2008). Molecular outflows are intimately associated with accretion disks and are therefore a strong indication that star formation is taking place in a clump. Class II Methanol masers (Menten 1991) are thermally pumped and require the presence of high densities and a strong mid-infrared radiation source and so are thought to be associated exclusively with high-mass protostellar objects (Minier *et al.* 2003; Breen *et al.* 2013) and dense gas (Urquhart *et al.* 2015; Billington *et al.* 2019). Water masers are collisionally pumped and, when encountered in star formation environments, are thought to be excited in the cavities of molecular outflows.

The right panel of Figure 9 shows the cumulative distribution functions for the $L_{\rm bol}/M_{\rm fwhm}$-ratio of clumps associated with each of the four star formation tracers. Inspection of these curves reveals that the association rates increase as a function of evolution, and this trend holds even up to the HII region stage for all but the EGOs, where the association rate peaks at the YSO stage and then begins to decrease. The association rates for EGOs, water and methanol masers with clumps classified as quiescent are zero, which is consistent with their classification as starless (as suggested by the lack of a 70-μm point source). However, there is a significant fraction associated with molecular outflows, which is a strong indication that star formation is already underway in them.

https://doi.org/10.1017/S1743921323002326 Published online by Cambridge University Press

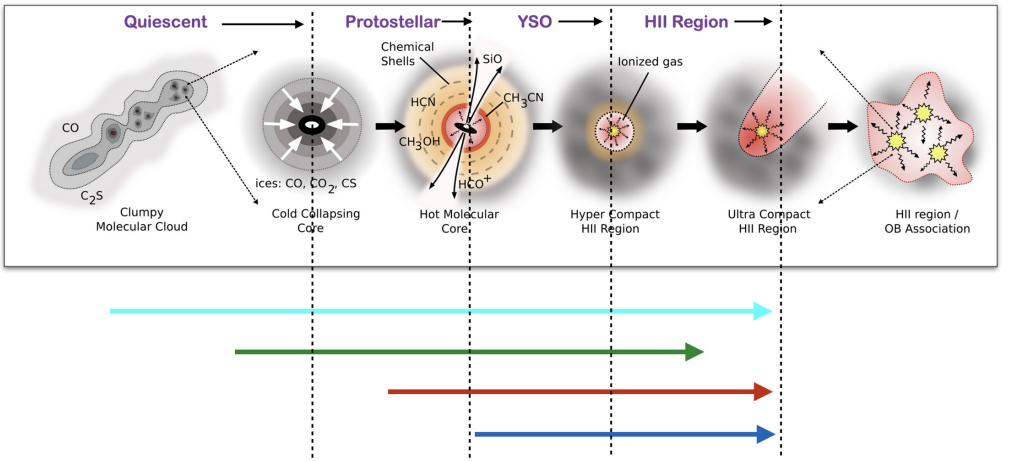

Figure 10. Schematic is the same as shown in Figure 1 but has been adapted to show approximately when the star formation tracers discussed in the text first appear and when they start to decline in frequency. The arrows correspond to outflows (top), EGOs (upper middle), water masers (lower middle) and methanol masers (bottom).

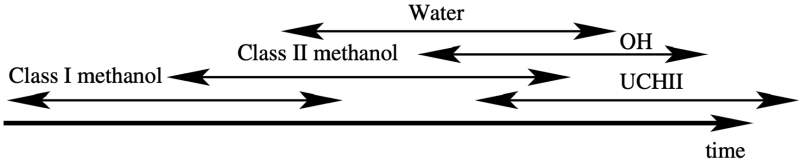

Figure 11. Model for an evolutionary sequence high-mass star formation regions constructed from maser emission. Image credit: This has been adapted from figure 2 of Ellingsen *et al.* (2007). Image Credit: Simon Ellingsen.

This analysis reveals that molecular outflows are the earliest signpost for star formation, followed by EGOs, and then by water and methanol masers (for more detailed analysis of methanol and water masers and star formation evolutionary sequences, see Breen *et al.* 2018; Billington *et al.* 2020; Ladeyschikov *et al.* 2020). Figure 10 presents a new version of the evolutionary schematic presented in Figure 1 that has been modified to indicate the approximate lifetimes that corresponds to the evolutionary stages of the four star formation tracers discussed in this section.

8. Masers as a Tool for Understanding Star formation

Another potentially useful probe to investigate the evolutionary sequence for high-mass stars is emission from maser transitions. Maser emission is ubiquitous in the Galaxy with different species being found to be attributed to specific physical processes, that in turn are associated with particular celestial objects (e.g., late-type stars, HII regions, star-forming regions; Elitzur 1992).

The first model for using a combination of maser transitions to construct an evolution sequence for high-mass star formation was proposed by Ellingsen *et al.* (2007). This was produced from the detection statistics obtained from OH, water and class I and class II methanol maser surveys (see Fig. 11 for schematic). This model was extended by Breen *et al.* (2010) with the incorporation of 12.2 GHz class II methanol maser transition and addition of relative lifetimes of the masers.

https://doi.org/10.1017/S1743921323002326 Published online by Cambridge University Press

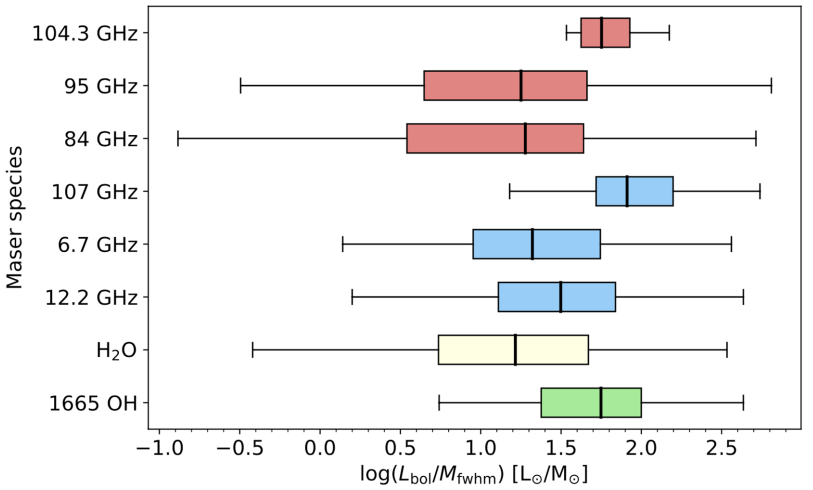

Figure 12. Box plot showing the distribution of $L_{\rm bol}/M_{\rm fwhm}$-ratios for ATLASGAL clumps associated with a wide range of masers species. This plot has been produced using the results from Ladeyschikov *et al.* (2022) and Yang *et al.* (2023) and appears in Yang *et al.* 2023 (this proceeding) and reproduced here with their permission. Image Credit: Wenjin Yang.

These early efforts to establish a reliable model using masers has been built upon in a series of recent studies that have combined results from maser surveys (e.g., HOPS Walsh *et al.* 2011, 2014, MMB Green 2009) and the $L_{\rm bol}/M_{\rm fwhm}$-ratio from ATLASGAL (Urquhart *et al.* 2018, 2022) as a measure of evolution. The first of these combined water, class II 6.7 and 12.2 GHz methanol and OH masers (Billington *et al.* 2020). This was followed by studies of 44 and 95 GHz class I methanol maser (Ladeyschikov *et al.* 2020) and water masers (Ladeyschikov *et al.* 2022). The range of maser species has recently been expanded again with the inclusion of the 84 and 104 GHz class I methanol masers and 107 GHz class II methanol maser (Yang *et al.* 2023).

Figure 12 presents a box plot that summarises all of these recent works. This shows there to be a lot of overlap between the different maser species but there are also significant differences with some maser species predominately associated with earlier evolutionary stages (e.g., 84 and 95 GHz class I methanol masers) while others are associated with more evolved stages (1665 MHz OH, 107 GHz class II methanol and 104.3 GHz class I methanol masers). Further work is needed to develop these results into a predictive model but the current work is promising.

9. Summary

The huge international effort to survey the Galactic plane at infrared, submillimetre and radio wavelengths have provided the large coverage necessary to identify large well-selected and representative samples of embedded high-mass star forming region, and start to develop an evolutionary sequence for high-mass star formation. In this review, we have given an overview of the progress that has been made over the past 20 years and how access to high-resolution far-infrared and submillimetre has allowed earlier evolutionary stages to be identified and their properties characterised.

The ATLASGAL has been used to produce a catalogue of dense high-mass clumps that includes examples of all embedded stages associated with high-mass star formation. This catalogue has been cross-matched with mid-infrared and radio surveys to produce a sample of ∼5000 clumps classified into one of four evolutionary stages; these being

https://doi.org/10.1017/S1743921323002326 Published online by Cambridge University Press

quiescent, protostellar, YSO and HII region. Comparing the luminosities and $L_{\rm bol}/M_{\rm fwhm}$-ratios for these four stages shows a clear trend with both parameters increasing with evolution, however, the cumulative distribution of these parameters is smooth and does not reveal any sharp jumps or discontinuities between the different evolutionary type. This suggests that star formation is a smooth and continuous process and that the evolutionary stages identified themselves do not represent fundamentally different stages or changes in the physical mechanisms involved.

The ATLASGAL $L_{\rm bol}/M_{\rm fwhm}$-ratio has been used as a measure of clump evolution to determine when other commonly used star formation tracers first appear and how long they persist for. This analysis has revealed that the appearance of a molecular outflow is the earliest manifestation of the star formation process, appearing before the formation of a detectable 70 μm point source, and persisting until after the formation of the HII region stage. Next to appear are the EGOs, which appear after the molecular outflow but still before the protostar becomes viable. The water and methanol masers are the last of the star formation tracers examined here to appear with the water masers appearing shortly before the methanol masers at approximate midway through the protostellar stage persisting until the appearance of the HII region. The $L_{\rm bol}/M_{\rm fwhm}$-ratio has also been used as a measure of evolution in a number of studies that focused on developing an evolutionary model based on different maser species that are associated with high-mass star formation. However, there is significant overlap between in the $L_{\rm bol}/M_{\rm fwhm}$-ratio distributions and although there is evidence that some maser species are more prevalent in the earlier stages and some in the more evolved stages.

Overall, significant progress has been made in recent years in constructing an evolutionary sequence and with surveys currently underway and new facilities coming on line the situation will undoubtedly improve in the coming years.

References

Aguirre J. E., Ginsburg A. G., Dunham M. K., *et al.* 2011, *ApJS*, 192, 4
Aumann H. H., Fowler J. W., and Melnyk M., 1990, *AJ*, 99, 1674
Beichman, C. A., Neugebauer, G., Habing, H. J., *et al.* 1988, Infrared astronomical satellite (IRAS) catalogs and atlases. Volume 1: Explanatory supplement, 1
Beuther H., Walsh A., Schilke P., *et al.* 2002, *A&A*, 390, 289
Beuther H., Bihr S., Rugel M., *et al.* 2016, *A&A*, 595, A32
Billington S. J., Urquhart J. S., König C., *et al.* 2019, *MNRAS*, 490, 2779
Billington S. J., Urquhart J. S., König C., *et al.* 2020, *MNRAS*, 499, 2744
Breen S. L., Ellingsen S. P., Caswell J. L., and Lewis B. E., 2010, *MNRAS*, 401, 2219
Breen S. L., Ellingsen S. P., Contreras Y., *et al.* 2013, *MNRAS*, 435, 524
Breen S. L., Contreras Y., Ellingsen S. P., *et al.* 2018, *MNRAS*, 474, 3898
Brunthaler A., Menten K. M., Dzib S. A., *et al.* 2021, *A&A*, 651, A85
Campbell B., Persson S. E., and Matthews K., 1989, *AJ*, 98, 643
Carey S. J., Noriega-Crespo A., Mizuno D. R., *et al.* 2009, *PASP*, 121, 76
Chan S. J., Henning T., and Schreyer K., 1996, A&AS, 115, 285
Churchwell E., Babler B. L., Meade M. R., *et al.* 2009, *PASP*, 121, 213
Clarke A. J., Lumsden S. L., Oudmaijer R. D., *et al.* 2006, *A&A*, 457, 183
Contreras Y., Schuller F., Urquhart J. S., *et al.* 2013, *A&A*, 549, A45
Cooper H. D. B., Lumsden S. L., Oudmaijer R. D., *et al.* 2013, *MNRAS*, 430, 1125
Csengeri T., Urquhart J. S., Schuller F., *et al.* 2014, *A&A*, 565, A75
Csengeri T., Leurini S., Wyrowski F., *et al.* 2016, *A&A*, 586, A149
Cyganowski C. J., Whitney B. A., Holden E., *et al.* 2008, *AJ*, 136, 2391
Davies B., Hoare M. G., Lumsden S. L., *et al.* 2011, *MNRAS*, 416, 972
de Villiers H. M., Chrysostomou A., Thompson M. A., *et al.* 2014, *MNRAS*, 444, 566
Dempsey J. T., Thomas H. S., and Currie M. J., 2013, *ApJS*, 209, 8

https://doi.org/10.1017/S1743921323002326 Published online by Cambridge University Press

Dokara R., Brunthaler A., Menten K. M., *et al.* 2021, *A&A*, 651, A86
Drew J. E., Greimel R., Irwin M. J., *et al.* 2005, *MNRAS*, 362, 753
Dzib S. A., Yang A. Y., Urquhart J. S., *et al.* 2023, *A&A*, 670, A9
Egan M. P., Price S. D., Kraemer K. E., *et al.* 2003, VizieR Online Data Catalog, 5114, 0
Elitzur M., 1992, *ARA&A*, 30, 75
Ellingsen S. P., Voronkov M. A., Cragg D. M., *et al.* 2007, in Chapman J. M., and Baan W. A., eds, Vol. 242, Astrophysical Masers and their Environments. pp 213–217 (arXiv:0705.2906), doi:10.1017/S1743921307012999
Faúndez S., Bronfman L., Garay G., *et al.* 2004, *A&A*, 426, 97
Gao Y., and Solomon P. M., 2004, *ApJS*, 152, 63
Giannetti A., Brand J., Sánchez-Monge Á., *et al.* 2013, *A&A*, 556, A16
Green J. A. a. a., 2009, *MNRAS*, 392, 783
Helfand D. J., Becker R. H., White R. L., *et al.* 2006, *AJ*, 131, 2525
Hill T., Burton M. G., Minier V., *et al.* 2005, *MNRAS*, 363, 405
Hoare M. G., Kurtz S. E., Lizano S., *et al.* 2007, Protostars and Planets V, pp 181–196
Hoare M. G., Purcell C. R., Churchwell E. B., *et al.* 2012, *PASP*, 124, 939
Ilee J. D., Wheelwright H. E., Oudmaijer R. D., *et al.* 2013, *MNRAS*, 429, 2960
Irabor T., Hoare M. G., Burton M., *et al.* 2023, *MNRAS*, 520, 1073
Jackson J. M., Rathborne J. M., Shah R. Y., *et al.* 2006, *ApJS*, 163, 145
Jackson J. M., Rathborne J. M., Foster J. B., *et al.* 2013, *PASA*, 30, 57
Kalcheva I. E., Hoare M. G., Urquhart J. S., *et al.* 2018, *A&A*, 615, A103
Kennicutt R. C., and Evans N. J., 2012, *ARA&A*, 50, 531
Kim W.-J., Wyrowski F., Urquhart J. S., *et al.* 2017, preprint, (arXiv:1702.02062)
König C., Urquhart J. S., Csengeri T., *et al.* 2017, *A&A*, 599, A139
Kroupa P., and Weidner C., 2003, *ApJ*, 598, 1076
Kruijssen J. M. D., and Longmore S. N., 2013, *MNRAS*,
Kurtz S., and Hofner P., 2005, *AJ*, 130, 711
Kurtz S., Churchwell E., and Wood D. O. S., 1994, *ApJS*, 91, 659
Ladeyschikov D. A., Urquhart J. S., Sobolev A. M., *et al.* 2020, *AJ*, 160, 213
Ladeyschikov D. A., Gong Y., Sobolev A. M., *et al.* 2022, *ApJS*, 261, 14
Lucas P. W., Hoare M. G., Longmore A., *et al.* 2008, *MNRAS*, 391, 136
Lumsden S. L., Hoare M. G., Oudmaijer R. D., and Richards D., 2002, *MNRAS*, 336, 621
Lumsden S. L., Hoare M. G., Urquhart J. S., *et al.* 2013, *ApJS*, 208, 11
Maud L. T., Moore T. J. T., Lumsden S. L., *et al.* 2015, *MNRAS*, 453, 645
McKee C. F., and Ostriker E. C., 2007, *ARA&A*, 45, 565
Medina S. N. X., Urquhart J. S., Dzib S. A., *et al.* 2019, *A&A*, 627, A175
Menten K. M., 1991, *ApJ*, 380, L75
Minier V., Ellingsen S. P., Norris R. P., and Booth R. S., 2003, *A&A*, 403, 1095
Minniti D., Lucas P. W., Emerson J. P., *et al.* 2010, New A, 15, 433
Molinari S., Brand J., Cesaroni R., and Palla F., 1996, *A&A* 308, 573
Molinari S., Pezzuto S., Cesaroni R., *et al.* 2008, *A&A*, 481, 345
Molinari S., Swinyard B., Bally J., *et al.* 2010, *A&A*, 518, L100
Moore T. J. T., Plume R., Thompson M. A., *et al.* 2015, *MNRAS*, 453, 4264
Motte F., Bontemps S., and Louvet F., 2018, *ARA&A*, 56, 41
Mottram J. C., Hoare M. G., Lumsden S. L., *et al.* 2007, *A&A*, 476, 1019
Murphy T., Mauch T., Green A., *et al.* 2007, *MNRAS*, 382, 382
Nguyen H., Rugel M. R., Menten K. M., *et al.* 2021, *A&A*, 651, A88
Nguyen H., Rugel M. R., Murugeshan C., *et al.* 2022, *A&A*, 666, A59
Ortiz-León G. N., Menten K. M., Brunthaler A., *et al.* 2021, *A&A*, 651, A87
Price S. D., Egan M. P., Carey S. J., *et al.* 2001, *AJ*, 121, 2819
Purcell C. R., Hoare M. G., Cotton W. D., *et al.* 2013, *ApJS*, 205, 1
Rosolowsky E., Hughes A., Leroy A. K., *et al.* 2021, *MNRAS*, 502, 1218
Schuller F., Menten K. M., Contreras Y., *et al.* 2009, *A&A*, 504, 415
Schuller F., Urquhart J. S., Csengeri T., *et al.* 2021, *MNRAS*, 500, 3064

Sevenster M. N., van Langevelde H. J., Moody R. A., *et al.* 2001, *A&A*, 366, 481
Skrutskie M. F., Cutri R. M., Stiening R., *et al.* 2006, *AJ*, 131, 1163
Sridharan T. K., Beuther H., Schilke P., *et al.* 2002, *ApJ*, 566, 931
Stil J. M., Taylor A. R., Dickey J. M., *et al.* 2006, AJ, 132, 1158
Thompson M. A., Hatchell J., Walsh A. J., *et al.* 2006, *A&A*, 453, 1003
Urquhart J. S., Busfield A. L., Hoare M. G., *et al.* 2007a, *A&A*, 461, 11
Urquhart J. S., Busfield A. L., Hoare M. G., *et al.* 2007b, *A&A*, 474, 891
Urquhart J. S., Busfield A. L., Hoare M. G., *et al.* 2008, *A&A*, 487, 253
Urquhart J. S., Hoare M. G., Purcell C. R., *et al.* 2009, *A&A*, 501, 539
Urquhart J. S., Morgan L. K., Figura C. C., *et al.* 2011, *MNRAS*, 418, 1689
Urquhart J. S., Moore T. J. T., Schuller F., *et al.* 2013a, *MNRAS*, 431, 1752
Urquhart J. S., Thompson M. A., Moore T. J. T., *et al.* 2013b, *MNRAS*, 435, 400
Urquhart J. S., Figura C. C., Moore T. J. T., *et al.* 2014a, *MNRAS*, 437, 1791
Urquhart J. S., Moore T. J. T., Csengeri T., *et al.* 2014b, *MNRAS*, 443, 1555
Urquhart J. S., Csengeri T., Wyrowski F., *et al.* 2014c, *A&A*, 568, A41
Urquhart J. S., Moore T. J. T., Menten K. M., *et al.* 2015, *MNRAS*, 446, 3461
Urquhart J. S., König C., Giannetti A., *et al.* 2018, *MNRAS*, 473, 1059
Urquhart J. S., Wells M. R. A., Pillai T., *et al.* 2022, *MNRAS*, 510, 3389
Walsh A. J., Breen S. L., Britton T., *et al.* 2011, *MNRAS*, 416, 1764
Walsh A. J., Purcell C. R., Longmore S. N., *et al.* 2014, *MNRAS*, 442, 2240
Wheelwright H. E., Oudmaijer R. D., de Wit W. J., *et al.* 2010, *MNRAS*, 408, 1840
White G. J., Etxaluze M., Doi Y., *et al.* 2009, in Onaka T., White G. J., Nakagawa T., and Yamamura I., eds, Astronomical Society of the Pacific Conference Series Vol. 418, AKARI, a Light to Illuminate the Misty Universe. p. 67
Wienen M., Wyrowski F., Schuller F., *et al.* 2012, *A&A*, 544, A146
Wienen M., Wyrowski F., Menten K. M., *et al.* 2015, *A&A*, 579, A91
Wienen M., Wyrowski F., Menten K. M., *et al.* 2018, *A&A*, 609, A125
Williams J. P., and McKee C. F., 1997, *ApJ*, 476, 166
Wood D. O. S., and Churchwell E., 1989, *ApJS* 69, 831
Wu Y., Zhang Q., Yu W., *et al.* 2006, *A&A*, 450, 607
Wynn-Williams C. G., 1982, *ARA&A*, 20, 587
Yang A. Y., Thompson M. A., Urquhart J. S., and Tian W. W., 2018, *ApJS*, 235, 3
Yang A. Y., Urquhart J. S., Thompson M. A., *et al.* 2021, *A&A*, 645, A110
Yang W., Gong Y., Menten K. M., *et al.* 2023, arXiv e-prints, p. arXiv:2305.04264

https://doi.org/10.1017/S1743921323002326 Published online by Cambridge University Press